Coupled phenomena in soil: Examples of insights gained from multi-physics particle-scale simulations

Catherine O'Sullivan [1,*], *José* Salomon[1], *Yongxin* Wang[1], *Tokio* Morimoto[2], *Mai* Sawada[3], and *Yohei* Nakamichi[4]

[1]Department of Civil and Environmental Engineering, Imperial College London, London SW7 2AZ, United Kingdom
[2] Department of Civil Engineering, The University of Tokyo, Tokyo, Japan
[3] School of Environment and Society, Institute of Science Tokyo (formerly Tokyo Institute of Technology), Tokyo, Japan
[4] Geotechnical Engineering Department, Obayashi Corporation, Tokyo Japan

Abstract. Arguably the most important idea in modern soil mechanics is the principle of effective stress put forward by Karl Terzaghi just over a century ago in 1923. The transformational impact of this principle on soil mechanics and geotechnical engineering reflects both the importance and challenge of accounting for the interaction between the solid and liquid phases in soil and other particulate materials. Apart from the multi-phase nature of soil, the influence of temperature changes and chemistry may also be significant. A comprehensive model should account for thermal, hydraulic, mechanical and chemical couplings. Despite significant advances our fundamental understanding of the interaction between the phases and phenomena remains incomplete, compromising our ability to accurately model or predict behaviour for engineering design analyses. Discrete element method (DEM) simulations, coarse-grained molecular dynamics, pore-network-modelling, and finite volume method computational fluid dynamics simulations together can advance understanding of key coupled phenomena in sand and clay. Emerging challenges include liquid-particle interactions considering both Newtonian and non-Newtonian fluids, the impact of pore-fluid chemistry on clay behaviour, the response of granular materials to changes in temperature, and the challenge of accurately modelling the pressure field when the pore-space includes multiple fluid phases. This paper demonstrates the value of particle and sub-particle scale simulations, while also introducing some of the numerical techniques that can be adopted to develop fully coupled simulation tools.

1 Introduction

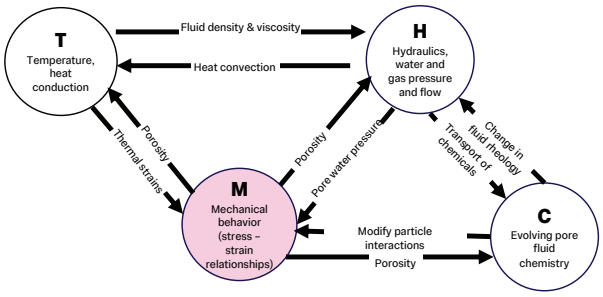

Fig. 1. Conceptual diagram of coupling in soil mechanics, modified from Gens [2]

The granular mechanics community is well acquainted with phenomenological responses that emerge from the particulate nature of granular materials including stress dependent-strength and stiffness, volumetric strains under shear distortion, non-linearity, non-coaxiality, etc. (e.g. Cundall [1]). The idea that the effective stress, i.e. the applied stress minus the pore water pressure, governs strength and deformation of soil is a crucial concept that is a cornerstone of soil mechanics. Fluid particle interaction has received some attention, particularly in the development of coupled discrete element method (DEM) – computational fluid dynamics (CFD) coupling. However, a number of recent seminal publications in geotechnical engineering, most notably Gens [2] have taken a broader perspective and identified 4 different types of coupling as illustrated schematically in Fig. 1. These are hydro-mechanical, thermo-mechanical, hydro-chemical, and chemo-mechanical. Climate change and the emergence of geothermal engineering have given impetus to advance understanding of coupled behaviour and particle-scale analyses and simulations play a key role in this. From an engineering perspective, capturing the mechanical behaviour is key in developing solutions. Adopting a core focus on mechanical behaviour, this paper considers three types of coupling, hydro-mechanical coupling, thermo-mechanical coupling and chemo-mechanical coupling. Results from a number of studies, each motivated by different applications are presented. In some cases we show how clear answers can be obtained from particle-scale simulations, in others the focus is more on tool development, and the required insighted into the fundamental mechanisms. The common theme is that particle-scale simulation can provide a unique insight to advance understanding which can directly or indirectly lead to innovation in geotechnical engineering.

* Corresponding author: cath.osullivan@imperial.ac.uk

2 Hydro-mechanical coupling

Hydro-mechanical coupling has achieved significant attention in the DEM modelling community which has long considered the development of coupled DEM-CFD simulation frameworks. In geomechanics there is scope to advance knowledge via fully resolved simulations of fluid flow, unresolved simulations of fluid flow, and pore network modelling. While contributions including Che et al. [3] and Knight et al. [4] have considered key issues to address to deliver unresolved coupled DEM-CFD simulations, this discussion focuses on fully resolved CFD simulations (sub-pore scale resolution – Sections 2.1 and 2.2), pore network modelling (pore-scale resolution – Section 2.3) and simulating undrained /partially drained responses by controlling volumetric strain (i.e. neither accounting for local variations in fluid pressure nor explicitly considering the fluid phase – Section 2.4). While these examples are arguably disparate, they have been selected to show that particle-scale and sub-particle scale simulation can be applied to study key areas of soil mechanics where uncertainty on mechanical behaviour remains.

2.1 Fully resolved non-Newtonian fluid flow

Within the geotechnical engineering community understanding of fluid flow in soil is underpinned by Darcy's law which assumes a constant fluid viscosity. However, for some applications the fluid viscosity can vary with shear rate, e.g. in the case of polymer fluids which can be used support deep excavations (Lam and Jefferis [5]). Polymer fluids exhibit a shear thinning rheology, i.e. their apparent viscosity (η_a) decreases with shear strain rate ($\dot{\gamma}$) and their η_a-$\dot{\gamma}$ relationship can be described by the Carreau model:

$$\frac{\eta_a-\eta_\infty}{\eta_0-\eta_\infty} = \left[1+\left(\lambda\dot{\gamma}\right)^2\right]^{(n-1)/2} \quad (1)$$

where η_0 is the viscosity at low fluid strain rates, i.e. the upper Newtonian plateau, η_∞ is the viscosity at high fluid strain rates, i.e. the lower Newtonian plateau, n determines the power-law exponent and λ is a time constant. The complexity of the rheology has contributed to the poor uptake of polymer fluids in excavation support applications in geotechnical engineering. Taking a packed bed of particles on a lattice packing (Fig. 2) so that symmetry can be exploited to reduce the computational cost) Wang et al. [6] used the OpenFOAM [7] CFD code to simulate the flow of polymer fluids. The CFD mesh which comprised about 1.5 million cells, was selected in verification simulations using water that compared predicted energy loss values to the analytically generated data in Zick and Homsy [8]. An innovative approach to choosing the sphere radii enabled a direct comparison with the experimental data in Ejezie et al. [9]. As illustrated in Fig. 3, the data from these simulations showed that the fluid-particle interaction forces experienced when polymers permeate granular materials with intrinsic permeabilities equivalent to the sands considered by Ejezie et al. can be up to 10^4 times the forces imparted by water at the same flow rate. These data are tangible evidence supporting the use of these fluids in excavation support. These results show the benefit of fully resolved simulations to give fluid-particle interaction data in emerging areas of interest in geotechnical engineering. An unresolved approach assumes a fluid-particle interaction model rather than informing us as to what the fundamental expressions. These models use pre-developed empirical or semi-empirical expressions whose application may be limited to specific flow regimes, particle size distributions or packing densities. In contrast the emergence of the fluid-particle interactions from fully resolved simulations means that they are a very useful way to inform understanding.

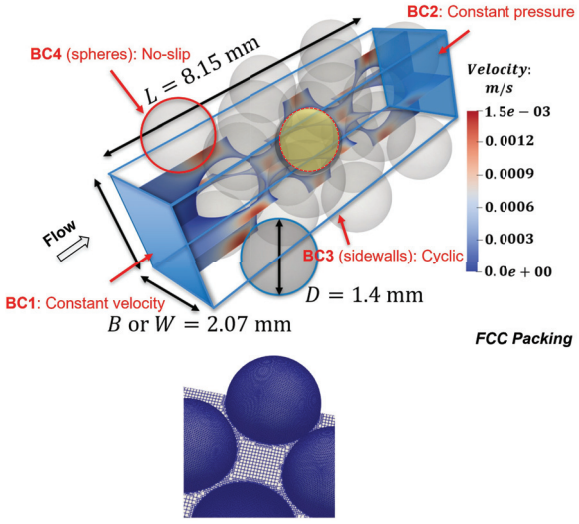

Fig. 2. Illustration of lattice packing used in CFD simulations with the Carreau model; with illustration of CFD mesh inset

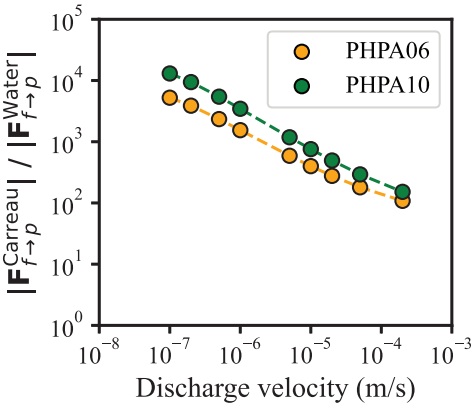

Fig. 3. Variation in fluid-particle interaction force with fluid discharge velocity for two concentrations of polymer (Modified after Wang et al. (2025))

2.2 Advancing understanding of capillary rise

Understanding the behaviour of unsaturated or partially saturated soil in which there is a mixture of air and water in the void space presents a significant challenge to the geotechnical engineering community. The complexity

of the mechanical response of unsaturated soil surpasses that of dry or fully saturated soil. One example of the complexity is the non-unique relationship between suction (negative or tensile pore water pressure) and degree of saturation that is captured in water retention curves (WRCs). This relationship differs during wetting and drying, and scanning curves link the so-called wetting and drying curves further adding to the complexity. As illustrated in Fig. 4 high resolution CFD simulations using OpenFOAM [7] can be used to simulate wetting and drying when the suction at the base of an assembly of regular spheres is systematically varied (Sawada et al. [10]). These simulations allow examination of the fundamentals of unsaturated soil mechanics. For example, the data on Fig. 5 show how the effect of the soil-water contact angle on water retention can be explored. These data also show that key features of physical WRCs can be captured even if the same contact angle is used in both drying and wetting.

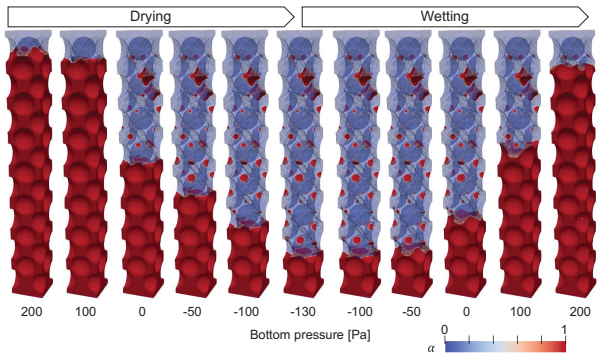

Fig. 4. Illustration of drying and wetting simulation in a FCC assembly of uniform spheres, red shading indicates fluid phase, blue shading indicates air phase

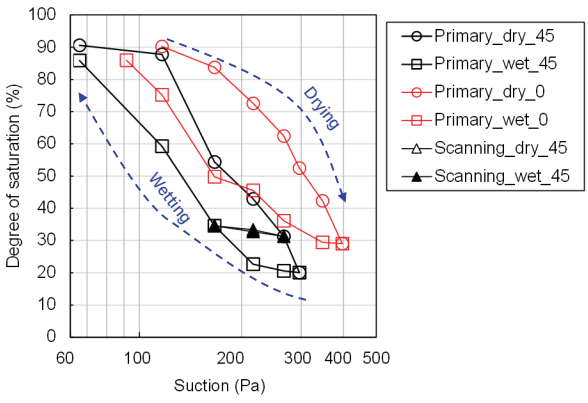

Fig. 5. Water retention curves emerging from the simulations, data for systems with contact angles of 0° and 45° (after Sawada et al. [10])

2.3 Pore-Network Modelling

Pore network models (PNMs) are well-established as a tool to study fundamental fluid flow in rock for petroleum engineering applications (e.g. Bryant and Blunt [11]). Pore network models give data on a scale that is larger than the fully resolved simulation and they have significant potential for upscaling from unresolved simulations. Chareyre et al. [12] demonstrated the potential to use PNMs to simulate flow in granular materials and obtain fluid-particle interaction forces. Fig. 6 schematically shows that in a PNM the granular material is portioned using a Delaunay-type triangulation and that the Voronoi-weighted pore centres, which form the nodes in the PNM, are located at the tetrahedra centroids. The PNM edges connect the nodes, and these represent the pore throats or constrictions in a physical material. The key equation in the model is based on Darcy's law and given as:

$$Q_{ab} = g_{ab}(p_a - p_b) \quad (2)$$

where Q_{ab} is the flow rate from pore a to pore b, g_{ab} is the conductance, and p_a and p_b are the pressures in pores (nodes) a and b respectively. Considering conservation of mass, a global system of simultaneous linear equations can be formed and solved to obtain the flow along each edge and pressure at each node.

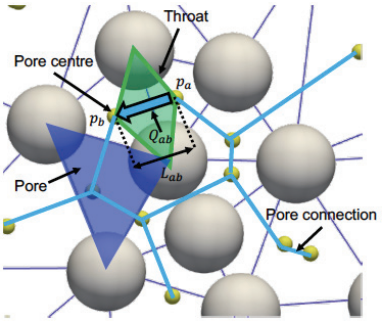

Fig. 6. Schematic illustration of PNM (Modified after Morimoto et al. [13])

The conductance term in Eq. 2 can be further reduced to more fundamental parameters as

$$g = \frac{\Gamma}{L\eta_f} \quad (3)$$

where L is the length of the edge connecting the nodes, η_f is the fluid viscosity and Γ is a function of the pore throat geometry.

The Hagen-Pouseille equation has previously been used to define Γ. Morimoto et al. [14] considered flow through lattice packings of uniform spheres at different packing densities to develop a refined expression for Γ:

$$\Gamma = 4\,\alpha_{ER-HR}\,\pi\,r_{eff}^2\,r_h^2 \quad (4)$$

where r_{eff} is the effective radius of the pore throat, r_h is the hydraulic radius, and α_{ER-HR} is shown in Fig. 7 to be a function of ξ where ξ which is a measure of the volume:surface area relation of pore throat is given by

$$\xi = \frac{\theta_{ab}^{1/3}}{\gamma_{ab}^{1/2}} \quad (5)$$

where θ_{ab} is the volume of fluid in the throat, γ_{ab} is the surface area of the particle in contact with the fluid in the throat. The efficacy of using this expression for Γ in a PNM is illustrated in Fig. 8 which compares the fluid-particle interaction forces acting on particles in a sample of polydisperse spheres calculated using high resolution direct numerical simulation with forces predicted using data from a PNM and expressions in Chareyre et al. [12].

Excellent agreement is obtained between the computationally expensive fully resolved simulation and the relatively simple PNM. These data support the development of refined conductance models to advance the use of PNM in coupled particle-fluid simulations. Morimoto et al. [14] showed that the fluid-particle interaction forces predicted using this PNM approach are more accurate than those obtained using the semi-empirical expressions typically adopted in unresolved DEM-CFD coupled simulations.

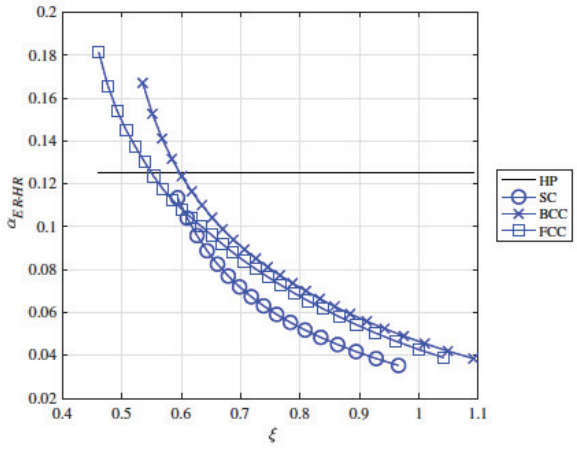

Fig. 7. Variation of $\boldsymbol{\alpha_{ER-HR}}$ with $\boldsymbol{\xi}$ for lattice packings of uniform spheres using data in Zick and Homsy [8]

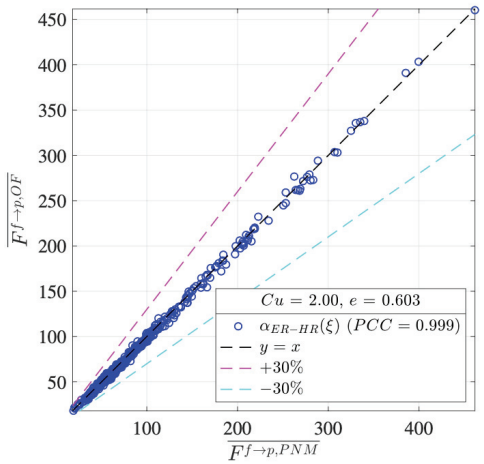

(b)

Fig. 8. Fluid particle interaction force determined from high resolution OpenFOAM [7] simulations versus fluid particle interaction force using conductance expression that incorporates $\boldsymbol{\alpha_{ER-HR}(\xi)}$ expression using data in Fig. 7 – polydisperse sample with a coefficient of uniformity of 2.0.

2.4 Uncoupled modelling of soil liquefaction

Static and earthquake induced liquefaction of loose sand or sand-like deposits (e.g. mine tailings) are a significant hazard. Understanding of liquefaction in geotechnical engineering has developed considering fully undrained (constant volume) response, DEM can be used to study liquefaction without explicit consideration of the fluid phase by restricting the system to deform at a constant volume (Ng and Dobry [15]). However, Salomon et al. [16] showed that the servo-controlled algorithms used to simulate soil mechanics element tests in DEM (e.g. Thornton [17]) can be adapted to simulate scenarios where limited drainage / dissipation of excess pore water pressure is permissible. The simulation process developed by Salomon et al. requires an initial simulation of triaxial compression of the sample under fully drained conditions to establish the drained volumetric strain. Then, the partially drained simulations are achieved by controlling the specimen volumetric strain to be a certain fraction (β) of the drained response. As illustrated in Fig. 9, the data generated show that a sample which liquefies (i.e. where the deviator stress q goes to zero) under undrained conditions, will not experience flow liquefaction if only 5% of the drained volumetric stress is allowed. These data support the development of technologies that exploit drainage to reduce liquefaction susceptibility. They also can advance the development of constitutive models to capture the partially drained response of soil adjacent to offshore wind turbine foundations.

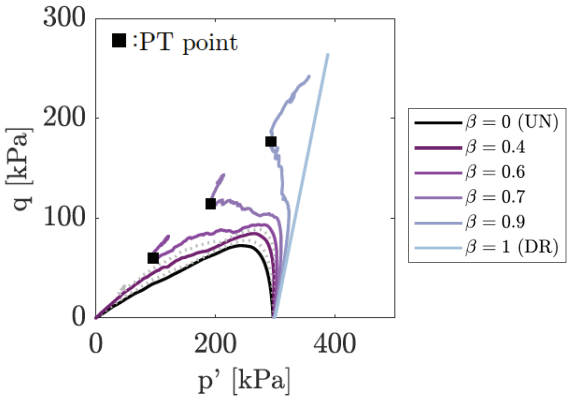

Fig. 9. Deviator stress ($\boldsymbol{q}$) versus mean effective stress ($\boldsymbol{p'}$) for drained, partially drained and undrained simulations of an assembly of frictional polydisperse spheres (Salomon et al. [16])

3 Thermomechanical coupling

Soil exhibits a highly complex thermomechanical behaviour. For example, as demonstrated in Baldi et al. [18]), in contrast to other materials which exhibit thermal expansion upon heating, the application of heat can cause a reduction in volume. Two key aspects of thermal response that need to be considered in developing DEM models are discussed here: (1) thermal expansion and conduction in the particle phase and (2) fluid advection and fluid- particle heat transfer. Radiation is not considered important at the temperatures currently encountered in geotechnical engineering applications.

3.1 Thermal response of the solid phase

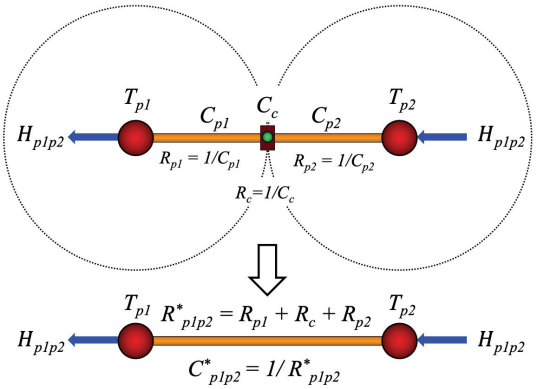

Fig. 10. Schematic illustration of two nodes and one edge in a heat pipe network used to simulate heat conduction in a granular material (after Morimoto et al. [19])

The use of heat pipe networks to simulate heat conduction in granular materials is outlined in Yun and Evans [20] & Dai et al. [21] and the basic principle is schematically shown in Fig. 10. Thermal nodes are located at the particle centroids. Flow between adjacent thermal nodes is given by and expression that is somewhat similar to Eq. 2:

$$\dot{Q}^T_{p1p2} = -C^*_{p1p2}\left(T_{p1} - T_{p2}\right) \quad (6)$$

where $\dot{Q}^T_{p1p2}$ is the heat flux along the heat network edge connecting particle $p1$ and particle $p2$, C^*_{p1p2} is the effective thermal conductivity, calculated following Bachelor and O'Brien [22], and T_{p1}, T_{p2} are the temperature at the centroids of particles $p1$ and $p2$.

Morimoto et al [19] used a heat pipe model to link the effective thermal conductivity tensor for a system of particles, k^*_{ij}, to the material fabric:

$$k^*_{ij} = k^{\beta*}_{ij} + k^{h*}_{ij} \quad (7)$$

Where $k^{\beta*}_{ij}$ is a function of coordination number and void ratio and k^{h*}_{ij} is a function of void ratio. Recognising that the Young's modulus, E is also a function of coordination number and void ratio, Morimoto et al. [19] used DEM simulations to explore a correlation between $k^{\beta*}_{ij}$ and E. Morimoto et al. generated a set of DEM samples with different void ratios and fabric anisotropies by compressing the samples isotropically (IC), in one-dimension (K0), subjecting the sample to a load-unload in triaxial compression (TCUL) and a load-unload in triaxial extension (TEUL). As illustrated in Fig. 11, despite the differences in fabric and initial void ratio of these samples, the effective thermal conductivity $k^{\beta*}_{zz}$ normalized by the pore fluid thermal conductivity, k_f, has a clear correlation with the product of E_z and the normal stress, σ_{zz}.

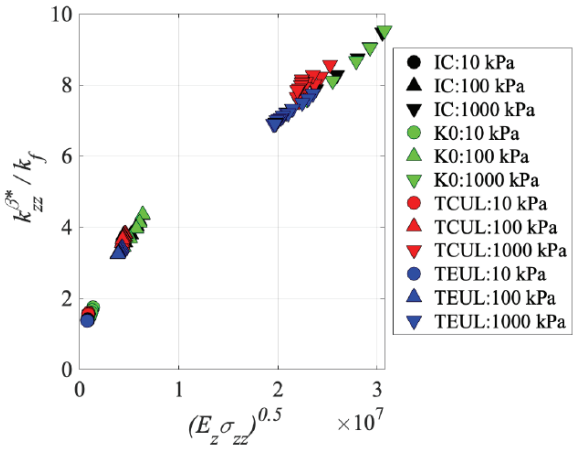

Fig. 11. Variation in coordination-number-dependent component of the effective thermal conductivity (tensor) with E_z , the system Young's modulus in the z direction

3.2 Fluid convection and fluid-particle heat transfer

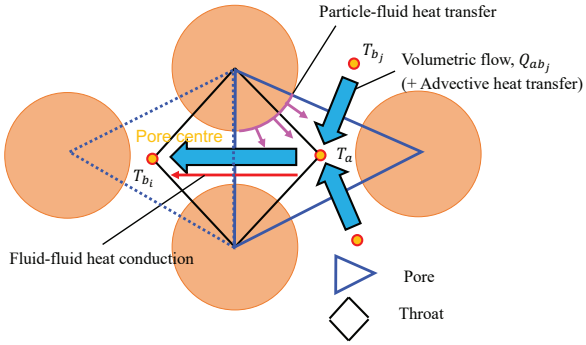

Fig. 12. Illustration of advective and conductive heat transfer in fluid phase and fluid-particle heat transfer (Morimoto [23])

The data presented in Fig. 11 neglect fluid flow. As illustrated in Fig. 12, a more comprehensive model should account for advective heat transfer and particle-fluid heat transfer. (Heat radiation is not important for the temperature ranges of interest in geotechnical engineering). The heat transport coefficient which is the mean heat flux/temperature difference can be related to the Nusselt number, Nu. Morimoto et al. [24] took the Nu formulation for flow in a non-circular pipe as a basis for developing an empirical expression. The Peclet number (Pc) is used to characterize heat transfer mechanisms in a fluid and calculation details are given in Morimoto et al. [24]. Fig. 13 compares Nu data obtained from OpenFOAM simulations and Nu values calculated using a modified form of the Nu expression in Muzychka and Yovanovich [25] for $Pc = 150$ considering an assembly of slightly polydisperse spheres. While there is some scatter in the data, these data support using equations such as those in Muzychka and Yovanovich to simulate fluid-particle heat transfer in the case of advective flow.

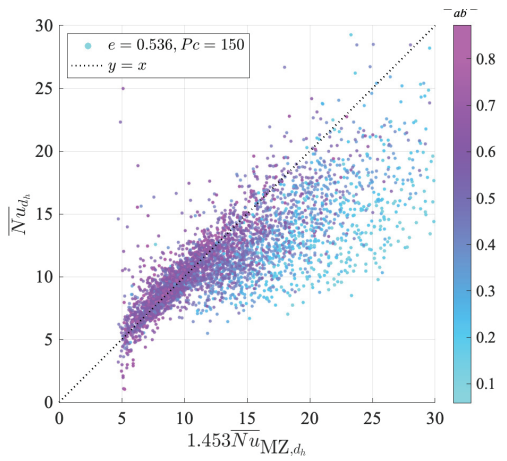

Fig. 13. Illustration of advective and conductive heat transfer in fluid phase and fluid-particle heat transfer

4 Chemo-mechanical coupling

In geotechnical engineering where particle size is used to define the soil type, clay is associated with particles less than 2 microns. These particles are flat and platy and the behaviour depends on the specific clay mineralogy. Clay behaviour poses a significant challenge in geotechnical engineering.

Clay particles are sufficiently small that the surface chemistry influences their mechanical behaviour. The pore water chemistry in turn impacts the surface chemistry. For example, as highlighted in Gens [2], Di Maio [26] demonstrated that Ponza bentonite will exhibit significant volumetric contraction when exposed to a saline pore fluid. Pagano et al. [27] introduce the various article-scale modelling strategies that can be applied to simulate the mechanical behaviour of clay. Nakamichi [28] used Coarse-Grained Molecular Dynamics (CGMD) (which is algorithmically similar to DEM) to numerically explore the response of kaolinite to changes in pore fluid pH and salt content. Kaolinite (sometimes termed China clay because of its use in ceramics) is a clay with low activity that has been very often used in fundamental geotechnical research.

Derjaguin-Landau-Vervey-Overbeek theory [29, 30] (DLVO) has a number of limitations, but it can be applied to model the interaction of kaolinite particles (Bandera et al. [21]). This theory can be used to calibrate interaction models for implementation in CGMD. In CGMD interactions are typically modelled using potential functions which give the interaction energy (U) as a function of particle separation (h). The interaction force is then given as $F = -\frac{dU}{dh}$. The Gay-Berne potential function (Gay and Berne [32]) (which is a generalization of the Lennard Jones potential for ellipsoidal particles), or variants of this potential function can be calibrated to capture the values of U predicted via DLVO theory.

4.1 Influence of pH on the mechanical response of kaolinite

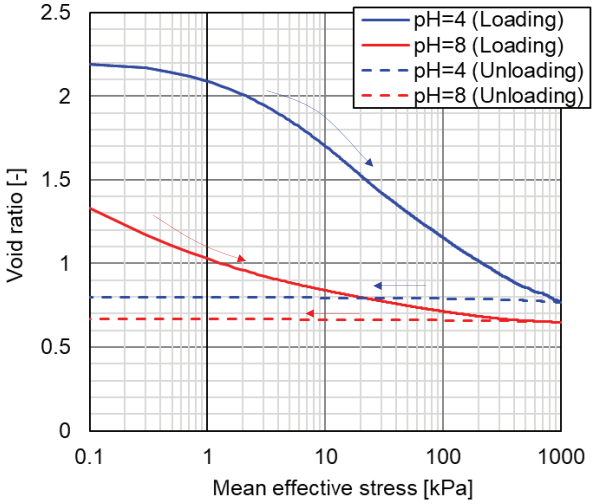

Fig. 14. Illustration of loading and unloading for isotropic compression of 10,648 kaolinite particles simulated using CGMD (see Nakamichi et al. [33])

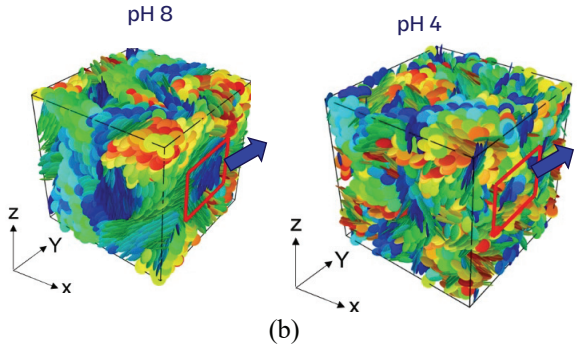

Fig. 15. Sample assembly following isotropic compression to 0.1kPa (see Nakamichi et al. [33])

A kaolinite particle comprises a stacked assembly of alumina and silica sheets. Consequently, for kaolinite particles 6 interaction combinations are possible, considering the silica face, the alumina face and the edges. The surface charge on kaolinite particles is highly dependent on pH. At pH=8 each interaction includes a positive local maximum in the interaction energy (an energy barrier) at short interaction distances (where $U = U_{eb}$ and $h = h_{eb}$) causing a large repulsive force for separations with $h < h_{eb}$. In contrast, for low pH values, e.g. pH=4, there is a surface charge heterogeneity so that some interaction interaction scenarios repulsive forces develop and for other interaction scenarios the interaction is always attractive. To account for this charge / interaction anisotropy Nakamichi et al. [33] developed an orientation-dependent weighting function. This function was implemented within the LAMMPS MD code [34]. Fig. 14 illustrates the response observed in isotropic compression simulations considering 10,648 ellipsoidal particles with an aspect ratio of aspect ratio of 10 (diameter is 2000 nm and thickness is 200 nm). The sample with pH=8 is more compressible than the sample with pH=4; this agrees with experimental observations

(e.g. Pedrotti and Tarantino [35]). The differences in microstructure evident in Fig. 15 align with the differences observed in SEM images of equivalent (but 1-D compression) experiments by Pedrotti and Tarantino.

4.2 Influence of salt concentration on the mechanical response of kaolinite

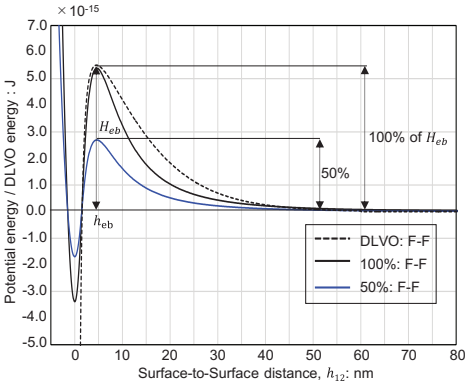

Fig. 16. Potential functions adopted in ideal simulations to look at the influence of pore fluid salt concentration on kaolinite

Referring to Israelachvilli [36], theoretically in the case of pH=8 the addition of salt to the pore fluid should reduce the surface charge, lower the magnitude of the interaction energy at the energy barrier and reduce the maximum repulsive force. Nakamichi (2025) explored this phenomenon using CGMD in a parametric study comparing one scenario where U_{eb}^{DLVO} was predicted using DLVO theory, and a second scenario where $U_{eb} = 0.5U_{eb}^{DLVO}$. Figure 16 compares the two potential functions used in the simulations, while Figure 17 shows that when the energy barrier is lowered, the void ratio at a given p' value is reduced. These observations broadly align with the experimental observations in Di Maio [26] and Tiwari and Ajmera [37].

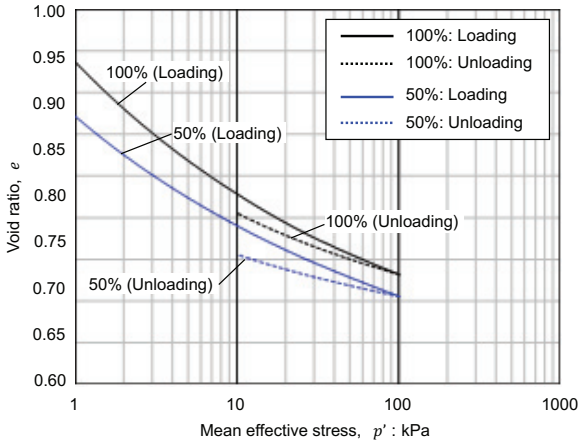

Fig. 17. Response in isotropic compression in terms of void ratio versus mean effective stress.

5 Conclusions and perspectives

The particulate nature of soil leads to complex response characteristics such as stress dependant strength and stiffness, volume change upon shear deformation, emergence of shear bands, etc. Additional complexity arises from the interaction of soil with the environment and changes in temperature, pore-water pressure / velocity and pore-water chemistry all contribute to this additional complexity. This contribution has indicated how a range of particle and sub-particle modelling techniques can advance understanding with the aim of improving predictions, reducing risk and developing innovative engineering solutions.

Acknowledgements

Jose Salomon's doctoral research was supported by ANID-Chile (grant #: 72210108) and an Imperial College Dixon Scholarship. Mai Sawada was supported by the Kajima Foundation's Researcher Exchange Support and the OBAYASHI Foundation. Yongxin Wang's doctoral research is supported by a Skempton Scholarship from the Department of Civil and Environmental Engineering, Imperial College London. Tokio Morimoto's doctoral research was funded by the European Union's Horizon 2020 research and innovation program Marie Skłodowska-Curie grant agreement MATHEGRAM No. 813202. Yohei Nakamichi's doctoral research was supported by OBAYASHI Corporation and an Imperial College Dixon Scholarship. All LAMMPS and OpenFOAM simulations were performed on the Imperial College Research Computing System facilities. (doi: 10.14469/hpc/2232).

References

[1] Cundall, P.A. A discontinuous future for numerical modelling in geomechanics?, Geotechnical Engineering Proceedings of the Institution of Civil Engineers, 149(1), 41-47, (2001).

[2] Gens, A. Soil–environment interactions in geotechnical engineering Géotechnique 60 (1), 3-74 (2010).

[3] Che, H., Windows-Yule, K., O'Sullivan, C. & Seville, J. A novel semi-resolved CFD-DEM method with two-grid mapping: Methodology and verification AIChE Journal, (2024).

[4] Knight, C., O'Sullivan, C., van Wachem, B. and Dini, D. Computing drag and interactions between fluid and polydisperse particles in saturated granular materials, Computers and Geotechnics 117, 103210. (2020).

[5] Lam, C. and Jefferis, S. Polymer Support Fluids in Civil Engineering. London, UK: ICE Publishing (2017).

[6] Wang, Y., Suo, S., Bortolotto, M. S., O'Sullivan, C., and Blunt, M. J. Particle-scale simulation of

polymer fluid permeation in sand International Journal of Geomechanics, In Press (2025).

[7] Open CFD. 2020. Open CFD Release OpenFOAM® v2012. [Online] Available at: https://www.openfoam.com/news/main-news/openfoam-v20-12.

[8] Zick, A. & Homsy, G. Stokes flow through periodic arrays of spheres. Journal of Fluid Mechanics. 115, 13–26. (1982).

[9] Ejezie, J.O., Jefferis, S.A., Lam, C., Sedighi, M., and Ahmad, S.M. Permeation behaviour of PHPA polymer fluids in sand. Géotechnique, 71(7), 561–570 (2021).

[10] Sawada, M., O'Sullivan, C., Tsiampousi, A., Salomon J. Insight into Hysteretic Drying and Wetting in Unsaturated Granular Soil from Fully Resolved Computational Fluid Dynamics Analysis Journal of Engineering Mechanics 151 (6), 04025018 (2025).

[11] Bryant, S. & Blunt, M. Prediction of relative permeability in simple porous media. Physical review A. 46 (4), 2004 (1992).

[12] Chareyre, B., Cortis, A., Catalano, E., & Barthélemy, E. Pore-scale modeling of viscous flow and induced forces in dense sphere packings. Transport in Porous Media, 94(2), 595-615. (2012).

[13] Morimoto, T., Zhao, B., Taborda, D.M.G. & O'Sullivan, C. Critical appraisal of pore network models to simulate fluid flow through assemblies of spherical particles Computers and Geotechnics 150, 104900 (2022).

[14] Morimoto, T., O'Sullivan, C., Taborda, D.M.G. Applying Network Modeling to Determine Seepage-Induced Forces on Soil Particles Journal of Geotechnical and Geoenvironmental Engineering 150 (5), 04024029 (2024).

[15] Ng, T.-T. and Dobry, R. Numerical Simulations of Monotonic and Cyclic Loading of Granular Soil. Journal of Geotechnical Engineering 120(2) 388-403 (1994).

[16] Salomon, J., Patino-Ramirez, F., O'Sullivan, C. Stress–dilatancy and micromechanics of sand under partially drained conditions Computers and Geotechnics 183, 107200 (2025).

[17] Thornton, C. Numerical simulations of deviatoric shear deformation of granular media, Géotechnique, Vol. 50, No. 1, pp. 43–53 (2000).

[18] Baldi, G., Hueckel, T., Peano, A., Pellegrini, R., Developments in modelling of thermo-hydro-geomechanical behaviour of Boom clay and clay-based buffer materials (vol. 2). Commission of the European Communities. Nuclear Science and Technology EUR 13365/2. (1991).

[19] Morimoto, T., O'Sullivan, C. & Taborda, D. M. G. Exploiting DEM to link thermal conduction and elastic stiffness in granular materials. Journal of Engineering Mechanics.148 (2), 04021139. (2022).

[20] Yun, T. S. & Evans, T. M. Three-dimensional random network model for thermal conductivity in particulate materials. Computers and Geotechnics. 37 (7-8), 991–998. (2010).

[21] Dai, W., Hanaor, D. & Gan, Y. The effects of packing structure on the effective thermal conductivity of granular media: A grain scale investigation. International Journal of Thermal Sciences. 142, 266–279. (2019).

[22] Batchelor, G. K. & O'Brien, R. Thermal or electrical conduction through a granular material. Proceedings of the Royal Society of London. A. Mathematical and Physical Sciences. 355 (1682), 313–333. (1977).

[23] Morimoto, T. Particle-scale numerical simulation of the thermal behaviour of granular materials. PhD Thesis Imperial College London. (2022).

[24] Morimoto, T., O'Sullivan, C., Taborda, D.M.G. Capturing particle-fluid heat transfer in thermo-hydro-mechanical analyses using DEM coupled with a pore network model Powder Technology 429, 118944, (2023).

[25] Muzychka, Y. S. and Yovanovich, M. M. Laminar Forced Convection Heat Transfer in the Combined Entry Region of Non-Circular Ducts, Journal of Heat Transfer, 126(1), pp. 54–61. (2004).

[26] Di Maio, C. Exposure of bentonite to salt solution: osmotic and mechanical effects. Géotechnique 46, No. 4, 695–707 (1996).

[27] Pagano, A.G., Alonso-Marroquin, F., Ioannidou, K., Radjai, F., O'Sullivan, C. Clay micromechanics: Mapping the future of particle-scale modelling of clay Proc. 8th International Symposium on Deformation Characteristics of Geomaterials (IS-Porto 2023) E3S Web of Conferences 544, 07009 (2024)

[28] Nakamichi, Y. Particle-Scale Simulation of Clay using Molecular Dynamics PhD Thesis Imperial College London. (2025)

[29] Derjaguin, B. V. and Landau, L. Theory of the stability of strongly charged lyophobic sols and of the adhesion of strongly charged particles in solution of electrolytes, Acta Physicochimica URSS 14, 633–662. (1941)

[30] Verwey, E. J. W. and Overbeek, J. T. G. Theory of the stability of lyophobic colloids. Amsterdam, Elsevier Inc. (1948)

[31] Bandera, S., O'Sullivan, C., Tangney, P. and Angioletti-Uberti, S. Coarse-grained molecular dynamics simulations of clay compression. Computers and Geotechnics, 138, 104333 (2021)

[32] Gay, J. G. and Berne, B. J., Modification of the overlap potential to mimic a linear site–site potential, Journal of Chemical Physics 74, 3316–3319 (1981).

[33] Nakamichi, Y., O'Sullivan, C., Tangney, P., Angioletti-Uberti, S. Modelling anisotropic surface charge of kaolinite particles depending on

pore water pH Computers and Geotechnics 173, 106505 (2024).

[34] Thompson, A. P., Aktulga, H. M., Berger, R., Bolintineanu, D. S., Brown, W. M., Crozier, P. S., in 't Veld, P. J., Kohlmeyer, A., Moore, S. G., Nguyen, T. D., Shan, R., Stevens, M. J., Tranchida, J., Trott, C. and Plimpton, S. J. Lammps - a flexible simulation tool for particle-based materials modeling at the atomic, meso, and continuum scales, Computer Physics Communications 271 (2022).

[35] Pedrotti, M. and Tarantino, A. An experimental investigation into the micromechanics of non-active clays, Geótechnique 68, 666–683 (2018).

[36] Israelachvili, J. N. *Intermolecular and Surface Forces*, 3rd Edition, Elsevier Inc. (2011).

[37] Tiwari, B. and Ajmera, B. Effects of Saline Fluid on Compressibility of Clay Minerals, Environmental Geotechnics, 1 (EG2), 108-120 (2014).

Notation

C^*_{p1p2}	Effective thermal conductivity at particle contact
CFD	Computational Fluid Mechanics
CGMD	Coarse-Grained Molecular Dynamics
DEM	Discrete Element Method
E	Young's modulus
$F_{F\to P}$	Fluid particle interaction force
F	Interaction force for clay particle interactions
g_{ab}	Conductance for edge connecting pore a and pore b
h	Separation distance for clay particle interactions
k^*_{ij}	Effective thermal conductivity (tensor)
L	Length of edge connecting nodes in a PNM
n	Determines the power-law exponent in the Carreau model
Nu	Nusselt number
p_a	Pressure in pore a
p_b	Pressure in pore b
$\boldsymbol{p'}$	Mean effective stress
Pc	Peclet number
PNM	Pore network model
Q_{ab}	Flow rate from pore a to pore b
$\dot{Q}^T_{p1p2}$	Heat flux along the heat network edge connecting particle $p1$ and particle $p2$
q	Deviator stress
r_{eff}	Effective pore radius
r_h	Hydraulic radius
T_{p1}, T_{p2}	Temperatures at the centroids of pore p1 and pore p2
U	Potential energy for clay particle interactions
WRC	Water retention curve
α_{ER-HR}	Term used to calculate geometrical contribution to conductance in a PNM
β	Fraction of drained volumetric strain allowed in partially drained DEM simulations
λ	time constant in Carreau model
η	Fluid viscosity
η_a	Apparent viscosity in Carreau model
η_0	Viscosity at low fluid strain rates – upper Newtonian plateau in Carreau model
η_∞	Viscosity at high fluid strain rates – lower Newtonian plateau in Carreau model
$\dot{\gamma}$	Fluid shear strain rate
Γ	Pore geometry contribution to conductance in a PNM
ξ	Volume:surface area relation of pore throat
Θ_{ab}	Volume of fluid in throat
γ_{ab}	Particle surface area in contact with fluid